RSC Advances

PAPER

View Article Online
View Journal | View Issue

Cite this: *RSC Adv.*, 2024, **14**, 38470

Manganese salophen covalently anchored to amino-functionalized graphene oxide as an efficient heterogeneous catalyst for selective epoxidation†

Robabeh Hajian * and Narjes Sadat Mousavi

Epoxidation of olefins catalyzed by manganese(III) salophen (MnSalop) immobilized on graphene oxide (GO) modified with 3-aminopropyltrimethoxysilane (GO·NH_2) has been reported. Characterization of the solid catalyst by FTIR, DR UV-Vis, FESEM, XRD, elemental scanning mappings, TGA/DTG, BET measurements, and ICP analysis aided in understanding the catalyst morphology. It confirmed that there was no significant demetallation or chemical change in MnSalop-GO·NH_2. The heterogeneous catalyst (MnSalop-GO·NH_2) showed high efficiency in the oxidation of different olefins with H_2O_2 as a green oxygen donor agent assisted by $NaHCO_3$ as co-catalyst at room temperature. The alkenes were oxidized to their corresponding epoxides with 88–100% selectivity and turnover frequency (TOF) values ranging from 40.7 to 162.8 h^{-1} in the presence of MnSalop-GO·NH_2 under mild conditions. When supported on GO, MnSalop-GO·NH_2 afforded epoxide yields comparable to those of the corresponding homogeneous analog. The prepared catalyst was selective for most olefins, with a high conversion. In addition, it could be reused four times without any remarkable loss in catalytic performance.

Received 20th July 2024
Accepted 12th November 2024

DOI: 10.1039/d4ra05280c

rsc.li/rsc-advances

1. Introduction

Catalytic olefin epoxidation is a valuable reaction for the synthesis of organic materials, as epoxides serve as chemical intermediates in the production of a wide range of commercial products, including epoxy paints, agrochemicals, and pharmaceutical products.[1,2] Consequently, there is a need to develop highly efficient catalysts for epoxidation reactions. Schiff base ligands have been the subject of intensive investigation because of their applications in various areas, including biological activities and coordination chemistry.[3] The biomimetic catalyst models of enzymatic monooxygenase and metal-Schiff base complexes have successfully oxidized olefins and other substances.[4,5] Numerous single oxygen donors, such as sodium periodate, alkyl hydroperoxide, hydrogen hydroperoxide, and iodosylbenzene, influence various oxidation processes.[6–9] Several catalytic systems have been previously reported for this purpose.[10] Metalloporphyrin and metal salen/salophen complexes have received notable attention because of their active redox systems, high catalytic activity, and selectivity.[11–15] Metal salophen successfully catalyzes the oxidation of various organic compounds.[16–18] Salophen, one of the most popular classes of tetradentate ligands, can be synthesized by condensing two equivalents of salicylaldehyde with one equivalent of 1,2-phenylenediamine derivative. Among various transition metals, manganese is particularly noteworthy and well-suited for alkene epoxidation due to its low toxicity and its presence in metalloenzymes.[19–23] Manganese salophen is a valuable and powerful catalyst for epoxidation.[24–26] Despite the high activity obtained with homogeneous catalysts, the aggregation of units through π–π interactions, difficulty in reusing the catalyst from the reaction medium, and self-destruction are several drawbacks of these systems.[27,28] One way to overcome these drawbacks is to immobilize the homogeneous catalyst on solid supports through encapsulation in a porous structure, covalent grafting, copolymerization, and buildup of the catalyst structure to produce polymers.[29–34] Graphene oxide (GO) compounds have been widely used in academic and industrial applications.[35,36] The oxygen-containing functional groups in two-dimensional graphene oxide structures, such as hydroxyl, epoxy, and carboxyl, lead to unique properties, including a high specific surface area, remarkable chemical stability, and intrinsic low mass.[37] Owing to the widespread flexibility in the design of composites, GOs can be tailored for various applications, including solar cells, catalysis, sensors, gas storage, and supports.[36,38–40] The functionalization of GO can enhance its capability to support the immobilization of various homogeneous compounds, such as metallic Schiff bases.[41,42] However, the covalent attachment of the catalyst on the surface of supports (GO) decreases the leaching of the catalyst

Department of Chemistry, Yazd University, Yazd 89195-741, Iran. E-mail: rhajian@yazd.ac.ir; Fax: +98-353-8210644; Tel: +98-353-31232822

† Electronic supplementary information (ESI) available. See DOI: https://doi.org/10.1039/d4ra05280c

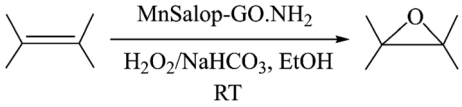

Scheme 1 Oxidation of olefins with H_2O_2/$NaHCO_3$ catalyzed by MnSalop-GO·NH_2.

during the reaction. Zarnegaryan *et al.* prepared a copper(II) Schiff base covalently anchored onto GO for the epoxidation of olefins.[43] Rayati *et al.* reported a Cu-Schiff base complex grafted onto a graphene oxide nanocomposite as an efficient and reusable catalyst for alkene oxidation.[44] Masteri-Farahani *et al.* functionalized graphene oxide and graphene oxide-magnetite nanocomposite with molybdenum-bidentate Schiff base complex for epoxidation of various alkenes.[45] Hassan *et al.* prepared a vanadium(IV) Schiff base amine-tagged graphene oxide composite to oxidize olefins.[46] Rezazadeh *et al.* synthesized Schiff base complexes of Mo(VI) immobilized on functionalized graphene oxide nanosheets for catalytic epoxidation of alkenes.[47] Rasoul Pour *et al.* immobilized the macrocyclic Schiff base copper complex on GO nanosheets and investigated its catalytic activity for olefins epoxidation.[48] As a part of our ongoing interest in developing heterogeneous catalytic systems for potential use in oxidative catalysts,[11,49,50] we have previously reported that $CoFe_2O_3$/Graphene Oxide can be appropriately used for supporting the Brominated Mn(III) Salophen.[51]

In this study, GO modified with 3-aminopropyltrimethoxysilane was prepared. Then, manganese(III) salophen was covalently attached to graphene oxide-bound amine (MnSalop-GO·NH_2). The immobilized manganese Schiff base was tested as a catalyst for the epoxidation of various alkenes in the presence of H_2O_2/$NaHCO_3$ in organic media. The catalyst recovery ability was also discussed (Scheme 1).

2. Experimental

2.1. Materials

All chemical materials were purchased from Fluka and Merck Chemical Company and used without further treatment. The chemical purities of all olefins were tested by gas chromatography and were confirmed to be higher than 98%. Manganese(III) salophen was prepared and characterized according to literature procedures.

2.2. Instrumental

FTIR spectra of the catalyst were recorded on Bruker FT-IR Equinox-55 instrument spectrophotometer, using pellets of the materials diluted with KBr. DR UV-Vis spectra were obtained using a V-670 spectrometer. FESEM of the samples were performed using a TE-SCAN MIRA (Czech) instrument. The pattern of X-ray diffraction (XRD) of compounds was taken on a D8 Advanced Bruker diffractometer using Cu-Kα radiation. The thermogravimetric and differential analysis (TG-DTG) was performed on STD Q600 in an N_2 atmosphere from 25 to 800 °C. Mn loading was performed using an ICP-Spectrociros CCD instrument. Adsorption–desorption isotherms were recorded on a BELSORB-mini II surface area analyzer at 77 K. The Brunauer–Emmett–Teller (BET) equation was calculated for specific surface area, and the Barrett–Joyner–Halenda (BJH) method was used for volume and pore diameter. The chemical products were analyzed by gas chromatography (Agilent 7890N, HP-5 19091 J-413 capillary column) with a flame ionization detector and *n*-decane as the internal standard using N_2 as the carrier gas.

2.3. Catalyst preparation

2.3.1. Synthesis of MnSalop. According to literature procedures, Manganese(III) salophen was prepared and characterized.[52] Salicylaldehyde (25 mmol) and 1,2-benzenediamine (12.5 mmol) were stirred in 30 mL of EtOH for 30 minutes. An ethanolic solution containing manganese(II) acetate tetrahydrate (5 mmol) was then added to the mixture and stirred for 2 hours. Subsequently, lithium chloride (7.5 mmol) was added, and the mixture was stirred for another 2 hours. The resulting Schiff base complex was filtered, washed with ethanol, and dried at room temperature for 24 hours.

2.3.2. Synthesis of GO. Graphene oxide was synthesized from graphite using a modified Hummers' method.[53] A mixture of 360 mL of 98% H_2SO_4 and 40 mL of H_3PO_4 was stirred, followed by the addition of 3 g of graphite powder. The mixture was then placed in an ultrasonic bath for 30 minutes to exfoliate the graphene oxide structure. Over 60 minutes, 18 g of $KMnO_4$ was added to the black suspension while stirring, allowing 10–15 minutes for complete dissolution of $KMnO_4$ and preventing a sudden rise in temperature or gas retention. After complete addition, the temperature was raised to 50 °C for 24 hours in a sand bath. Subsequently, ice cubes made from 400 mL of double distilled water were added to the mixture, causing the color of the solution to turn cherry red. By slowly adding about 5 mL of hydrogen peroxide (30% H_2O_2), the solution's color turned completely orange. After the complete removal of gas from the solution, the precipitate was separated using a centrifuge. Finally, the collected precipitate was washed with distilled water and ethanol and dried in an oven at 70 °C overnight.

2.3.3. Preparation of amino-functionalized GO (GO·NH_2). In the next step, GO was functionalized with 3-aminopropyltrimethoxysilane (APTMS), following a previously reported procedure.[54] Briefly, GO (1 g) was dispersed in toluene (30 mL) by ultrasonication for 30 min. APTMS (10 mmol) was added to the above mixture and refluxed under nitrogen gas for 24 h. The resultant product (GO·NH_2) was isolated by filtration, washed completely with ethanol to remove the unreacted residue of the silylating reagent, and dried under vacuum.

2.3.4. Preparation of manganese(III) salophen grafted GO (MnSalop-GO·NH_2). In the final step, GO·NH_2 (1 g) was suspended in toluene (20 mL) *via* sonication. Then, a manganese(III) salophen (0.25 g) solution in 10 mL of methanol was added to the above mixture and refluxed for 24 h to yield MnSalop-GO·NH_2. The product was separated and washed three times with EtOH before drying under a vacuum.

2.4. Catalytic test

In a typical experiment, alkene (0.5 mmol) in 4 mL solvent, MnSalop-GO·NH_2 catalyst (100 mg), hydrogen peroxide as a green oxidant (5 mmol; 30%), and sodium bicarbonate (0.5 mmol) were mixed and stirred at ambient conditions for the appropriate time. The progress of the reaction was followed by GC equipped with an FID detector and an HP-5 column (*n*-decane as the internal standard). After completion of the reaction, the MnSalop-GO·NH_2 catalyst was separated by centrifugation, washed with EtOH, dried carefully, and recycled for the next run.

3. Results and discussion

3.1. Characterization of MnSalop-GO·NH_2

As described in Scheme 2, GO was prepared by oxidative exfoliation of graphite in the first step. GO was treated with 3-aminopropyltrimethoxysilane (APTMS) in refluxing toluene for 24 h. On the other hand, APTMS can be grafted onto GO for its –COOH, –OH, and epoxy groups to form Si–O linkages. Subsequently, Mn(III) salophen can interact with GO·NH_2 through covalent bonds.

3.1.1. ICP analysis. The MnSalop loading was calculated from the manganese content in MnSalop-GO·NH_2 analyzed by ICP. The MnSalop loading was calculated based on the manganese content in MnSalop-GO·NH_2, as determined by ICP analysis. The results indicated that the loading amount of MnSalop in MnSalop-GO·NH_2 was estimated to be 0.37 mmol g^{-1}.

3.1.2. DR UV-Vis studies. The DR UV-Vis spectra of GO, MnSalop, and MnSalop-GO·NH_2 is shown in Fig. 1. GO showed no characteristic absorption bonds in the UV-Vis region (Fig. 1a). The characteristic absorption peak at 475 nm for MnSalop is attributed to the d–d transitions of manganese(III) salophen (Fig. 1b).[55] This absorption (with low intensity and red shift) was detectable in the spectrum of the MnSalop-GO·NH_2, confirming the attachment of manganese(III) salophen to the

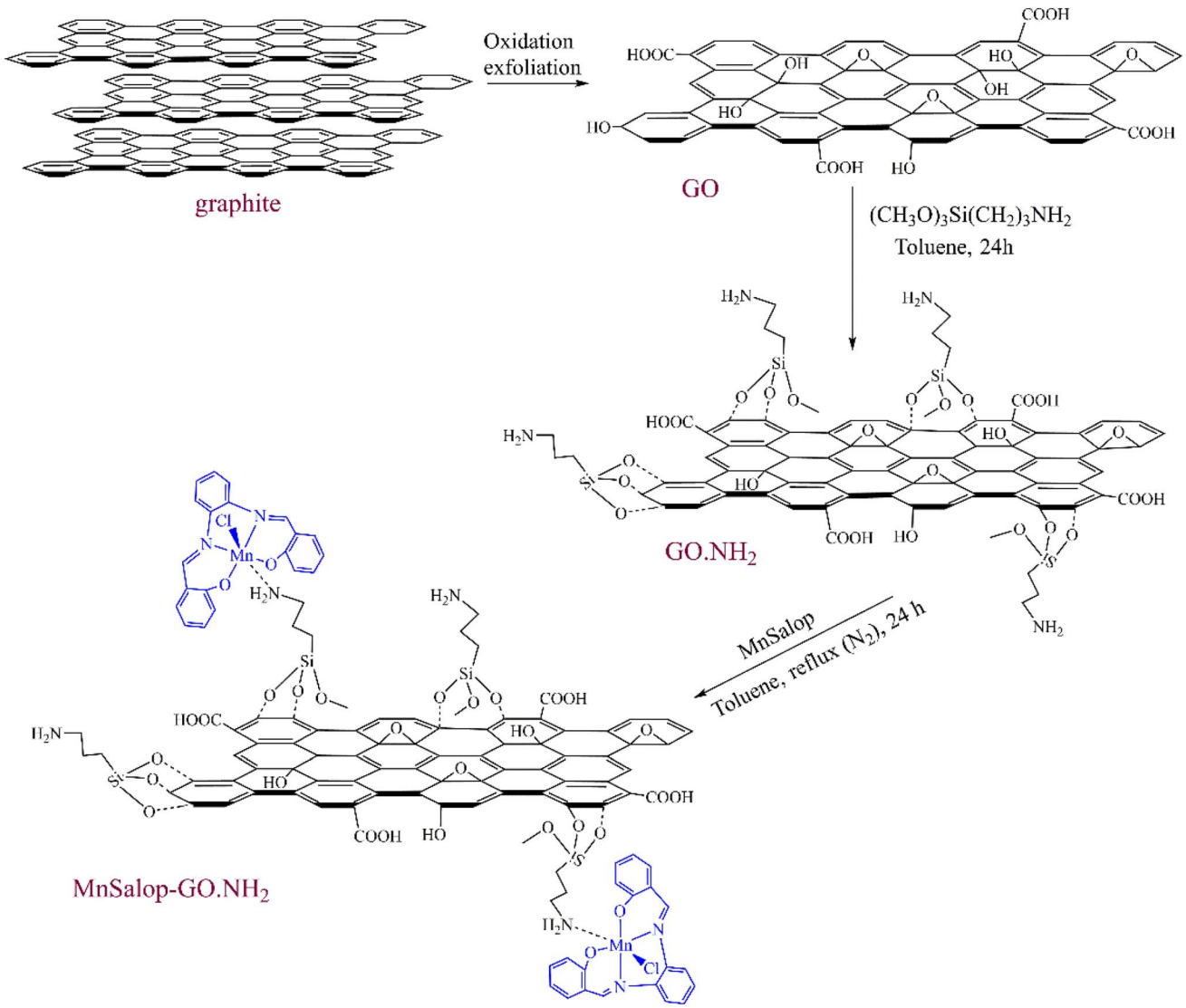

Scheme 2 Schematic illustration for the preparation of MnSalop-GO·NH_2.

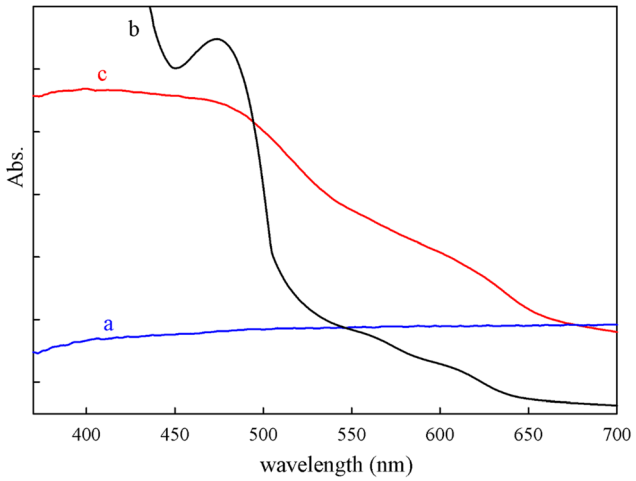

Fig. 1 DR UV-Vis spectra of: (a) GO, (b) MnSalop and (c) MnSalop-GO·NH_2.

surface of the modified GO (Fig. 1c). The red shift observed might be attributed to the interaction between the carbonyl and hydroxyl groups of GO and the manganese salophen complex.[44]

3.1.3. IR studies. Fig. 2 represents the FT-IR spectra of GO, GO·NH_2, MnSalop, MnSalop-GO·NH_2, and recovered MnSalop-GO·NH_2. The vibrational bands of functional groups such as C–O (epoxy; 1040 cm^{-1}), C=O (carboxyl; 1733 cm^{-1}), C–OH (hydroxyl groups; 1224 cm^{-1}), and C=C (aromatic ring; 1628 cm^{-1}) can be observed in the IR spectrum of pure GO (Fig. 2a).[53] The strong bands at 1090 cm^{-1} and 996 cm^{-1} correspond to the stretching vibrations of Si–O–Si and Si–O–C, respectively, indicating the silylanization of GO through chemical bonding. Two bonds around 3443 and 1520 cm^{-1} were attributed to the stretching and bending modes of N–H of amine-tagged graphene oxide (Fig. 2b).[46] A characteristic band at 1605 cm^{-1} appeared in the FT-IR spectrum of MnSalop, which corresponds to the stretching of the azomethine group (C=N) of the manganese Schiff base complex (Fig. 2c).[55] In the FTIR spectrum of MnSalop-GO·NH_2, the peak at 1603 cm^{-1} was attributed to the imine group (C=N) stretching in the manganese salophen molecule. Additionally, the stretching vibration bands of the silanol groups at 1092 and 1030 cm^{-1} and the band at 1530 cm^{-1} reveal amine groups. These results confirm the coordination of MnSalop to the amine-modified GO nanosheets (Fig. 2d).

3.1.4. FE-SEM, XRD and elemental mapping studies. The field transmission SEM image and size distribution histogram of MnSalop-GO·NH_2 are shown in Fig. 3a and b. A typical FESEM image shows a non-regular morphology; therefore, MnSalop-GO·NH_2 has an amorphous structure with an average size of 50 nm. The particle sizes ranged from 20 to 120 nm, as assigned. XRD pattern of GO and MnSalop-GO·NH_2 have been shown in Fig. 3c. For GO, the characteristic peak at $2\theta = 11.3°$ corresponds to the (001) reflection.[45,56] In the XRD pattern of MnSalop-GO·NH_2, the GO pattern did not disappear, indicating that the structure of GO was preserved after the immobilization of MnSalop. In addition, the XRD spectrum of MnSalop-

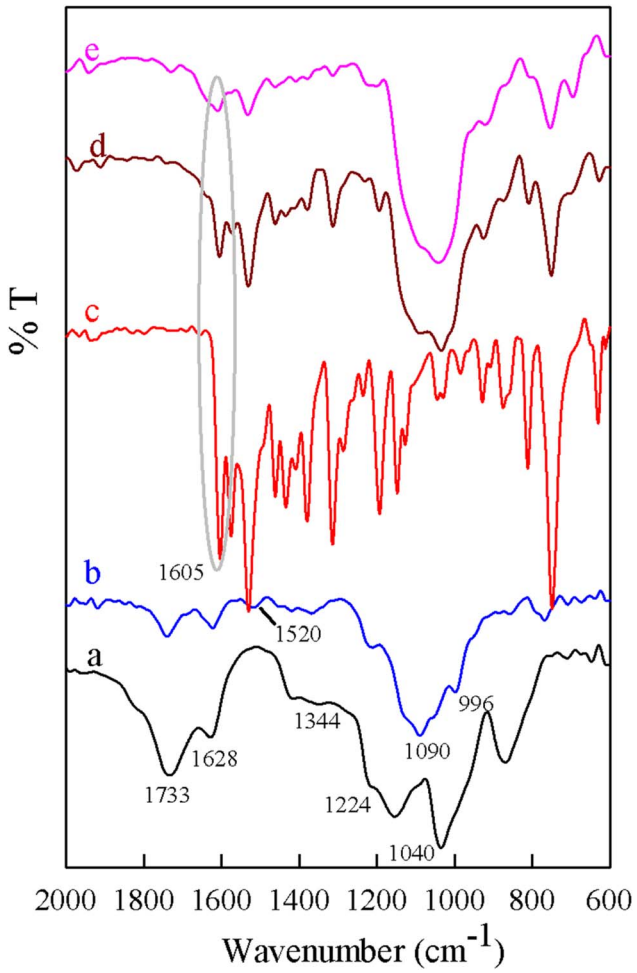

Fig. 2 FT-IR spectra of (a) GO, (b) GO·NH_2, (c) MnSalop, (d) MnSalop-GO·NH_2 and (e) recovered MnSalop-GO·NH_2.

GO·NH_2 exhibited a broad peak at $2\theta = 25.3°$, verifying that the important oxygen-containing groups of GO were modified, and this peak is the most significant signal for metal-Schiff base complexes.[43,47] The broadness of the diffraction peak is assigned to poor crystalline structure of compounds. The elemental mapping of the selected regions (Fig. 3d) in the MnSalop-GO·NH_2 texture displays the distribution of manganese, chloride, nitrogen, carbon, oxygen, and silicon on the synthesized catalyst surface (Fig. 3e–j). The results showed successful immobilization of the papered catalyst on the GO support.

3.1.5. TG-DTG studies. The TG-DTG profiles of MnSalop-GO·NH_2 was determined to study its thermal stability (Fig. 4). According to previous reports, GO exhibits multistep weight loss at temperatures ranging from 20 to 700 °C. The weight loss near 100 °C was due to the evaporation of physically adsorbed water, and the other remarkable weight loss was due to the pyrolysis of oxygen-carrying functionalities. TG-DTG curve for MnSalop-GO·NH_2 showed a three-step weight loss at temperatures ranging from 30 to 650 °C (76%). The first step of weight loss (10%) below 200 °C was ascribed to the evaporation of adsorbed water on the surface catalyst. The second step of weight loss occurs in the temperature range of 220–320 °C and

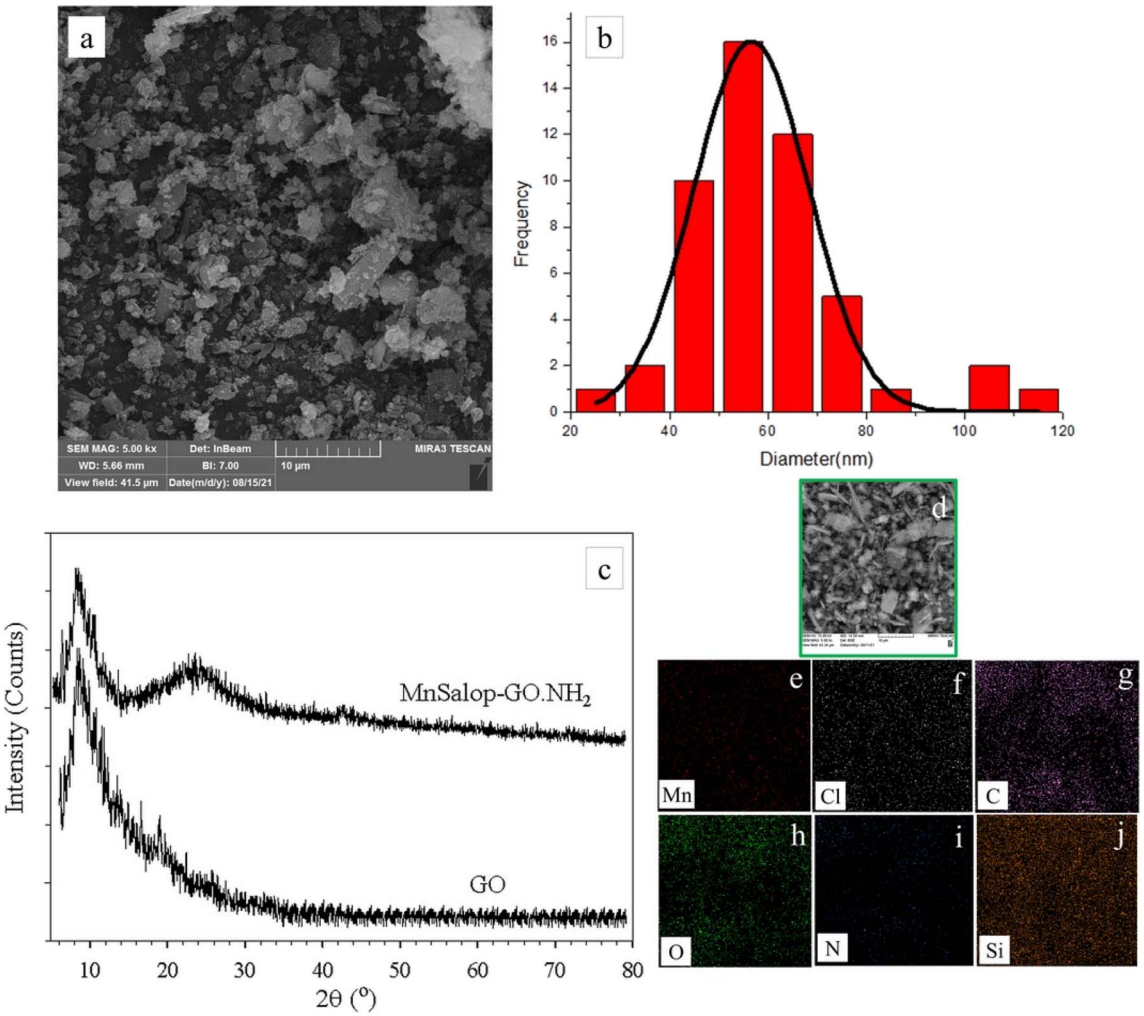

Fig. 3 (a) FE-SEM image of MnSalop-GO·NH_2, (b) histogram of the particle size of MnSalop-GO·NH_2, (c) XRD patterns of GO and MnSalop-GO·NH_2 and (d–j) elemental mapping image of the sample separated once.

is related to the oxidation of organic compounds (APTMS).[46] Removing carbon groups by reaction with oxygen to form CO_2 and CO gases is responsible for the 12% weight loss. The third significant weight loss (54%) over a vast 320–650 °C temperature range was due to the slow thermal decomposition of the manganese(III) salophen complex.

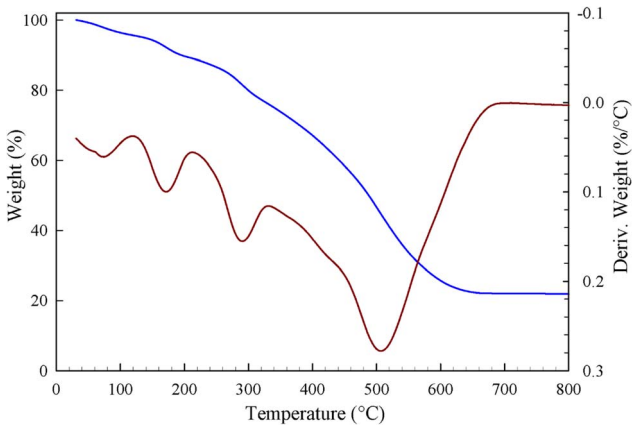

Fig. 4 TG-DTG curve for MnSalop-GO·NH_2.

3.1.6. N_2 adsorption–desorption studies. Nitrogen adsorption–desorption isotherms were obtained to investigate the textural properties of the MnSalop-GO·NH_2 (Fig. 5). The sorption isotherm is type IV with a hysteresis loop for mesoporous materials, according to the IUPAC classification. The specific surface area and total pore volume of the catalyst obtained with the BET method were 23 $m^2\ g^{-1}$ and 0.173 $cm^3\ g^{-1}$, respectively. The mean pore diameter of the catalyst was also found to be 7.99 nm according to the Barrett–Joyner–Halenda method.

3.2. Catalytic performance

3.2.1. Epoxidation of cyclooctene. The catalytic activity of the obtained MnSalop/clicked GO hybrid nanomaterial was evaluated for the epoxidation of alkenes using H_2O_2 as the oxidant. The data are shown in Fig. 6. To optimize the conditions for the model reaction, epoxidation of cyclooctene was examined by changing various parameters, including the catalyst dose, reaction time, oxidant, activator amount, and solvent

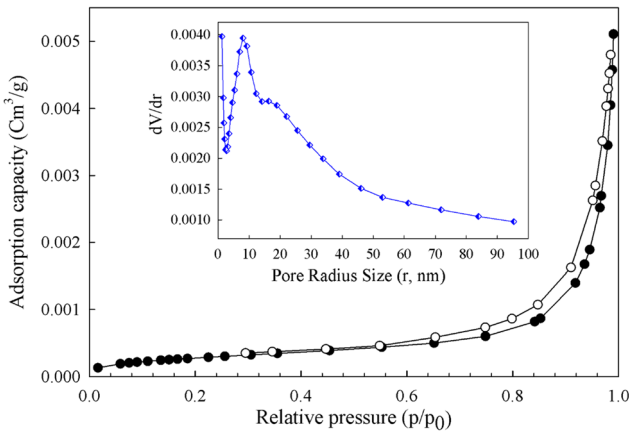

Fig. 5 N_2 adsorption isotherms and pore distribution of MnSalop-GO·NH_2.

type. Different amounts of MnSalop-GO·NH_2 catalysts were tested in the model reaction. By increasing the catalyst dosage from 50 to 100 mg, the conversion increased from 81 to 98%. A higher amount of the catalyst did not significantly affect the conversion under ambient conditions. The desired conversion was achieved when 100 mg (0.037 mmol) of MnSalop-GO·NH_2 was used. Only a small amount of product was detected in the absence of the prepared catalyst (Fig. 6a). The choice of an appropriate solvent for epoxidation is crucial because the solvent can potentially adsorb onto the catalyst's surface, thereby affecting the accessibility of olefins to the active sites. However, the solvent significantly affected the ionic and radical epoxidation mechanisms, influencing the rates, selectivity, and yield. In ionic mechanisms, polar solvents help stabilize charged intermediates, whereas in radical mechanisms, the solvent affects radical stability, diffusion, and termination processes. Various solvents, such as dichloromethane, methanol, acetone, acetonitrile, chloroform, and ethanol, have been investigated for the optimization of the reaction media in the epoxidation of cyclooctene with H_2O_2/$NaHCO_3$. High conversions were obtained using ethanol and acetonitrile as solvents. The higher catalytic performance in EtOH and CH_3CN can be attributed to the polarity of solvent and the solubility of

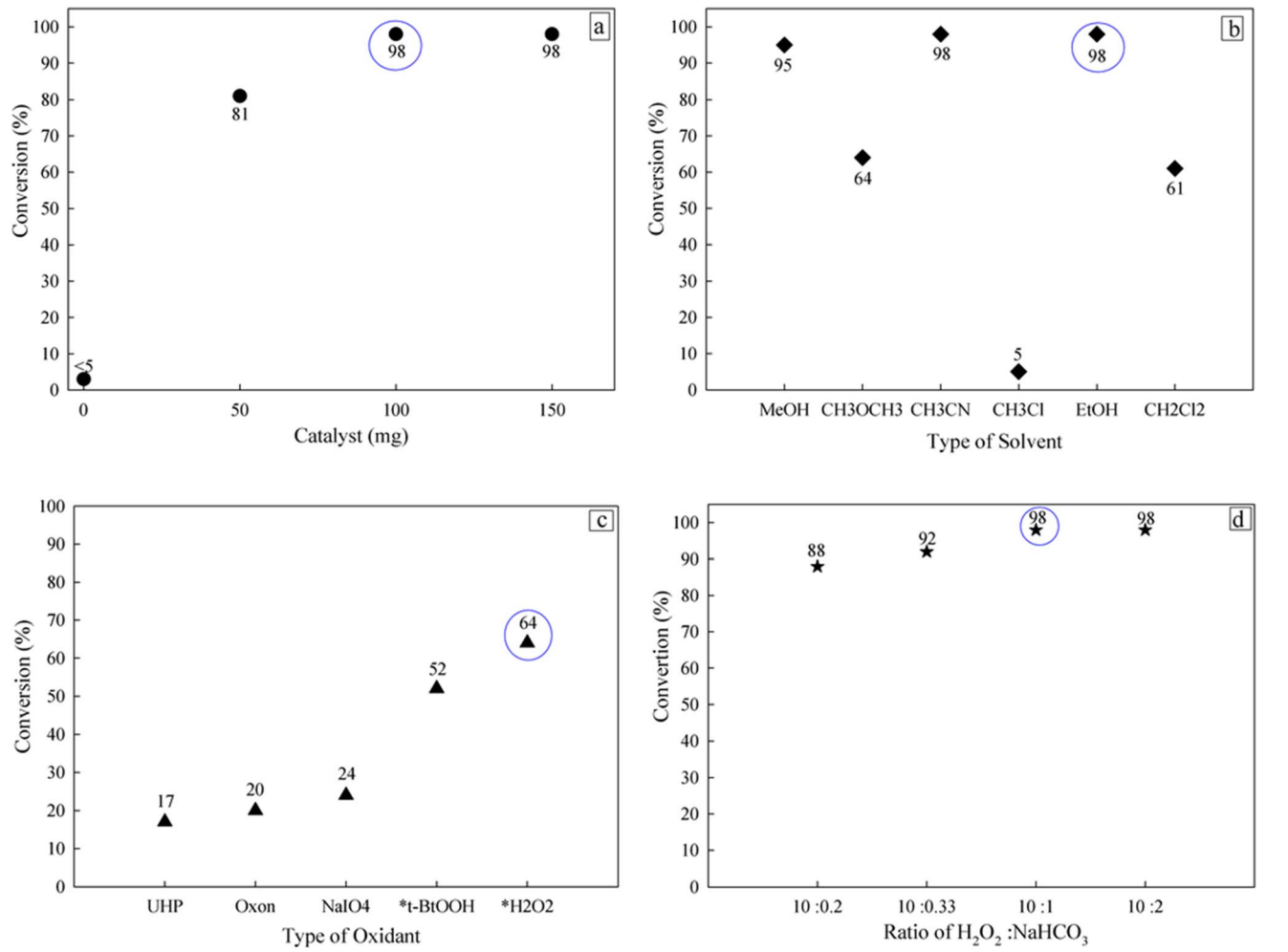

Fig. 6 The cyclooctene epoxidation by MnSalop-GO·NH_2 process under mild condition: (a) influence of catalyst dose, olefin : H_2O_2 : $NaHCO_3$ are (1 : 10 : 1); 5 min; solvent (4 mL), (b) influence of type of solvent, catalyst : olefin : H_2O_2 : $NaHCO_3$ are (2 : 27 : 270 : 27); 5 min; solvent (4 mL), (c) influence of type of oxidant, catalyst:olefin:oxidant are (2 : 27 : 54); 5 min; EtOH (4 mL); *(catalyst : olefin : oxidant, 2 : 27 : 270), (d) influence of ratios of H_2O_2/$NaHCO_3$, catalyst : olefin : H_2O_2 : $NaHCO_3$ are (2 : 27 : 270 : *X*); 5 min; EtOH (4 mL).

$NaHCO_3$ in this condition. However, ethanol was chosen as the optimal solvent because of its environmental compatibility (Fig. 6b). Oxygen donors such as urea hydrogen peroxide (UHP), sodium periodate, hydrogen peroxide, *tert*-butyl hydroperoxide, and oxone were also tested for epoxidation of olefins under reaction conditions. The highest oxidation product was obtained when H_2O_2 was used as the green oxidant. Among the different molar ratios of olefin/H_2O_2, a ten-fold equivalent of the oxygen donor was chosen as the optimized amount (Fig. 6c). The activation of H_2O_2 seriously depended on the presence of $NaHCO_3$ as the buffer medium *via* the formation of HCO_4^- ions.[57] To determine the influence of sodium bicarbonate on the performance of MnSalop-GO·NH_2, cyclooctene oxidation was performed using various H_2O_2/$NaHCO_3$ ratios. The maximum conversion of cyclooctene occurred at a 10 : 1 molar ratio of H_2O_2 to $NaHCO_3$ (Fig. 6d). Thus, sodium bicarbonate is an essential co-catalyst of the oxidation reaction.

The time courses of the control components of this heterogeneous system, including GO, GO·NH_2, MnSalop, and MnSalop-GO·NH_2 were also investigated under the same reaction conditions. The supporting materials (GO and GO·NH_2) exhibited low catalytic performances. The homogeneous catalyst (MnSalop) afforded a conversion of 94% after 5 min. The immobilization of MnSalop on the modified GO increased the conversion percentage (98% after 5 min) in the epoxidation reaction because of the isolation of the active sites of the GO solid (Fig. 7).

3.2.2. Epoxidation of different alkenes. It was having proved the catalytic performance of MnSalop-GO·NH_2 in the model system, the scope of the protocol was subsequently expanded to a range of alkenes, as shown in Table 1. According to the results of this table, the prepared heterogeneous catalyst exhibits high activity and selectivity in the epoxidation reaction. The amine ligand attached to graphene oxide occupies the sixth coordination position of manganese(III) salophen, which increases the catalytic activity due to its sigma-donating property. The oxidation reactions continued until no further progress was observed in the experiment. Cyclooctene was completely converted to its corresponding epoxide in 5 min with a 98% conversion (TOF 159.5 h^{-1}). Epoxidation of cyclohexene with 93% conversion and 88% epoxide selectivity, and cyclohexene-1-one and cyclohexene-1-ol were produced as two by-products (TOF 151.4 h^{-1}). In comparison, 1-octene and 1-hexene, as chain aliphatic olefins, exhibited lower activity, with the conversion of 25% (TOF 58.6 h^{-1}) and 36% (TOF 40.7 h^{-1}) with 100% selectivity due to increased steric hindrance. In the case of styrene, the major product was styrene epoxide with 88% conversion, and only small amounts of benzaldehyde were produced as minor products (TOF 143.3 h^{-1}). Epoxidation of α-methylstyrene with 92% conversion and 94% epoxide selectivity led to 6% of acetophenone as a by-product. The relatively high conversion of α-methylstyrene can be assigned to the increased electron density of the double bond (TOF 149.8 h^{-1}). The epoxidation of limonene proceeded with 100% epoxide selectivity (86% for 1,2-epoxide and 14% for 8,9-epoxide) and 72% conversion with a final TOF of 120.5 h^{-1}. The results of the epoxidation of α-pinene showed that epoxide was the major product of the oxidation process (90%), and only trace amounts of verbenone and verbenol compounds were by-products (TOF 162.8 h^{-1}).

To demonstrate the effectiveness of the heterogeneous catalyst, the TOF (h^{-1}) of this work (MnSalop-GO·NH_2) was compared with our previously reported system, CFeGO@MnSalBr[51] (Table S1†). A more detailed analysis of the results reveals that MnSalop-GO·NH_2 exhibits higher catalytic efficiency than the CFeGO@MnSalBr catalyst. This can be attributed to the reduced mobility of CFeGO@MnSalBr due to the presence of the magnetite core.

Based on Krishnan's ideas and other reports, a possible mechanism is proposed for the epoxidation of alkenes with H_2O_2/$NaHCO_3$ using a manganese complex. In this mechanism, HCO_4^- is a more active and nucleophilic oxidant than H_2O_2, which can coordinate with manganese metal and form an intermediate manganese-acyl peroxymonocarbonate complex or a high-valent Mn=O intermediate. The active atomic oxygen can be transferred from the molecule's intermediate to the C=C bond to form the epoxide (Scheme 3).[57,58]

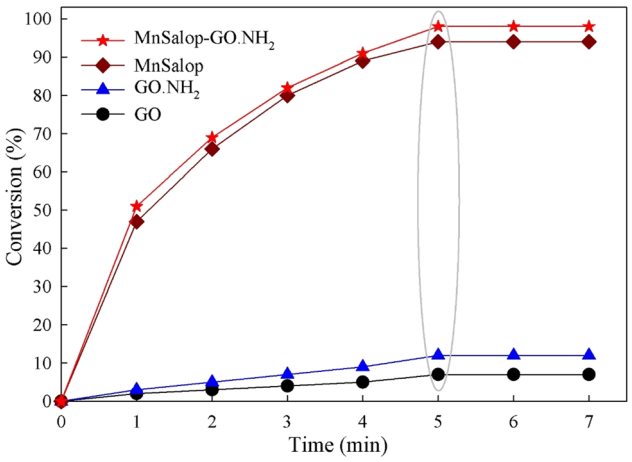

Fig. 7 Conversion–time curves for epoxidation of cyclooctene with GO, GO·NH_2, MnSalop and MnSalop-GO·NH_2. Reaction condition: the molar ratios for catalyst : olefin : H_2O_2 : $NaHCO_3$ are (2 : 27 : 270 : 27); GO and GO·NH_2 (100 mg); EtOH (4 mL).

3.3. The reusability of catalyst

The heterogenization of different catalysts is of great importance from an economical point of view and for environmentally friendly applications. Hence, the durability and reproducibility of MnSalop-GO·NH_2 as a heterogeneous catalyst in *cis*-cyclooctene epoxidation was studied. After completion of the reaction, the prepared catalyst was isolated by easy filtration from the reaction mixture, washed twice with ethanol, and then dried carefully before use in the subsequent run. After the fourth run, epoxidation conversion decreased from 98 to 77% (Fig. 8). In addition, atomic absorption spectroscopy was used to measure the amount of MnSalop leached. The results demonstrated that after the first two runs, no considerable Mn was detected (0.75% and 0.41%, respectively). The FT-IR spectra of MnSalop-GO·NH_2 were compared before and after the fourth run and

Table 1 Epoxidation of olefins with H_2O_2 catalyzed by MnSalop-GO·NH_2 after 5 min[a]

	Substrate	Product	Conversion[b] (%)	Epoxide selectivity (%)	TOF (h^{-1})
1		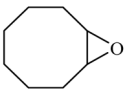	98	100	159.5
2		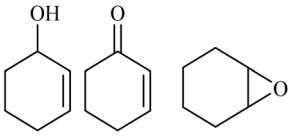	93	88	151.4
3	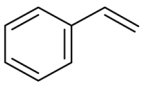	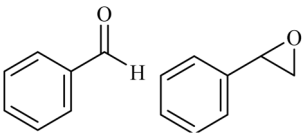	88	91	143.3
4	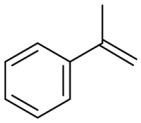	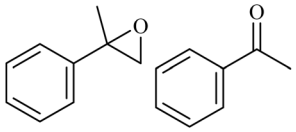	92	94	149.8
5	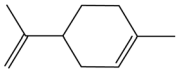	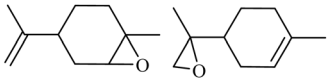	74	(86% exo), (14% endo)	120.5
6	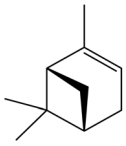	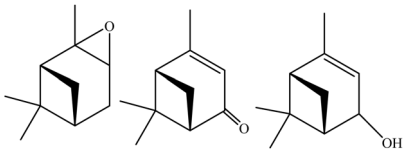	100	90	162.8
7	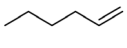	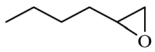	36	100	58.6
8	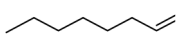	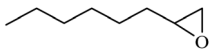	25	100	40.7

[a] Reaction conditions: the molar ratios for catalyst : olefin : H_2O_2 : $NaHCO_3$ are (2 : 27 : 270 : 27), EtOH (4 mL). [b] GC yield based on the starting olefin.

showed the same patterns (Fig. 2e), which emphasizes that this catalyst not only has good durability but also high reproducibility, instilling confidence in its application.

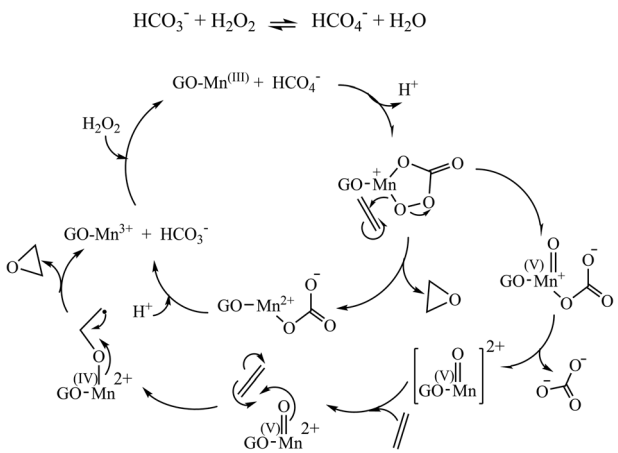

Scheme 3 Proposed mechanism for the epoxidation of alkene with H_2O_2/$NaHCO_3$ by MnSalop-GO·NH_2.

The heterogenization of different catalysts is of great importance from an economical point of view and for environmentally friendly applications. Hence, the durability and reproducibility of MnSalop-GO·NH_2 as a heterogeneous catalyst in *cis*-cyclooctene epoxidation was studied. After completion of

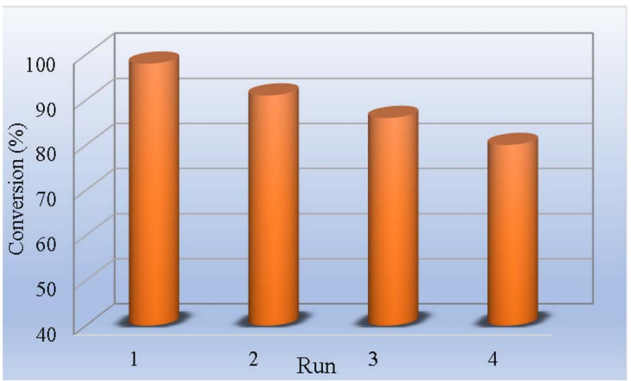

Fig. 8 Recycling data for MnSalop-GO·NH_2 as catalyst in the epoxidation of cyclooctene with H_2O_2 : $NaHCO_3$.

the reaction, the prepared catalyst was isolated by easy filtration from the reaction mixture, washed twice with ethanol, and dried carefully before use in the subsequent run. After the fourth run, epoxidation conversion decreased from 98% to 77% (Fig. 8). Also, atomic absorption spectroscopy was used to measure the amount of MnSalop leached. The results demonstrated that no considerable Mn was detected after the first two runs (0.75% and 0.41%). The FT-IR spectra of MnSalop-GO·NH_2 was compared before and after the fourth run and showed the same patterns (Fig. 2e), emphasizing that this catalyst has good durability and high reproducibility, instilling confidence in its application.

4. Conclusion

In this study, amine-functionalized graphene oxide was synthesized and used to support the immobilization of manganese(III) salophen chloride (MnSalop). The catalytic activity of the heterogeneous catalyst MnSalop-GO·NH_2 was evaluated in the epoxidation of various olefins using H_2O_2 as an eco-friendly oxidant and $NaHCO_3$ as co-catalyst in EtOH. This catalytic system offers several advantages, including mild reaction conditions, high selectivity, and acceptable reusability.

Data availability

All relevant data are within the manuscript and its additional files. The data are available from the corresponding author on reasonable request.

Conflicts of interest

There is no conflict of interest in the article.

Acknowledgements

We are thankful to the Yazd University Research Council for the partial support of this research.

References

1 C. Boulechfar, H. Ferkous, A. Delimi, A. Djedouani, A. Kahlouche, A. Boublia, A. S. Darwish, T. Lemaoui, R. Verma and Y. Benguerba, *Inorg. Chem. Commun.*, 2023, **150**, 110451–114062.
2 Y. Meng, F. Taddeo, A. F. Aguilera, X. Cai, V. Russo, P. Tolvanen and S. Leveneur, *Catalysts*, 2021, **11**, 765–840.
3 A. M. Abu-Dief and I. M. Mohamed, *Beni-Suef Univ. J. Basic Appl. Sci.*, 2015, **4**, 119–133.
4 H. Kargar, A. A. Ardakani, M. N. Tahir, M. Ashfaq and K. S. Munawar, *J. Mol. Struct.*, 2021, **1233**, 130112–130124.
5 A. Nishinaga and H. Tomita, *J. Mol. Catal.*, 1980, **7**, 179–199.
6 B. Bahramian, V. Mirkhani, S. Tangestaninejad and M. Moghadam, *J. Mol. Catal. A: Chem.*, 2006, **244**, 139–145.
7 N. H. Lee, J.-C. Byun and T.-H. Oh, *Bull. Korean Chem. Soc.*, 2005, **26**, 454–456.
8 V. Mirkhani, M. Moghadam, S. Tangestaninejad, I. Mohammadpoor-Baltork and N. Rasouli, *Catal. Commun.*, 2008, **9**, 2171–2174.
9 M. Sedighipoor, A. H. Kianfar, W. A. K. Mahmood and M. H. Azarian, *Inorg. Chim. Acta*, 2017, **457**, 116–121.
10 A. Nodzewska, A. Wadolowska and M. Watkinson, *Coord. Chem. Rev.*, 2019, **382**, 181–216.
11 R. Hajian, S. Tangestaninejad, M. Moghadam, V. Mirkhani and I. Mohammadpoor-Baltork, *J. Iran. Chem. Soc.*, 2016, **13**, 1061–1067.
12 O. Kocyigit and E. Guler, *J. Inclusion Phenom. Macrocyclic Chem.*, 2010, **67**, 29–37.
13 S. Tangestaninejad, M. Moghadam, V. Mirkhani, I. Mohammadpoor-Baltork and R. Hajian, *Inorg. Chem. Commun.*, 2010, **13**, 1501–1503.
14 Ş. Uysal and Z. E. Koç, *J. Mol. Struct.*, 2018, **1165**, 14–22.
15 A. Pappalardo, F. P. Ballistreri, R. M. Toscano, M. A. Chiacchio, L. Legnani, G. Grazioso, L. Veltri and G. Trusso Sfrazzetto, *Catalysts*, 2021, **11**, 465–474.
16 C. W. Anson, S. Ghosh, S. Hammes-Schiffer and S. S. Stahl, *J. Am. Chem. Soc.*, 2016, **138**, 4186–4193.
17 M. A. Asraf, C. I. Ezugwu, C. Zakaria and F. Verpoort, *Photochem. Photobiol. Sci.*, 2019, **18**, 2782–2791.
18 M. Salavati-Niasari, A. Badiei and K. Saberyan, *Chem. Eng. J.*, 2011, **173**, 651–658.
19 N. Sarkar, P. K. Bhaumik and S. Chattopadhyay, *Polyhedron*, 2016, **115**, 37–46.
20 M. Maiti, D. Sadhukhan, S. Thakurta, E. Zangrando, G. Pilet, A. Bauzá, A. Frontera, B. Dede and S. Mitra, *Polyhedron*, 2014, **75**, 40–49.
21 P. Kar, M. G. Drew and A. Ghosh, *Inorg. Chim. Acta*, 2013, **405**, 349–355.
22 R. Egekenze, Y. Gultneh and R. Butcher, *Polyhedron*, 2018, **144**, 198–209.
23 G. De Faveri, G. Ilyashenko and M. Watkinson, *Chem. Soc. Rev.*, 2011, **40**, 1722–1760.
24 M. A. Fardjahromi, M. Moghadam, S. Tangestaninejad, V. Mirkhani and I. Mohammadpoor-Baltork, *RSC Adv.*, 2016, **6**, 20128–20134.
25 S. Y. Liu and D. G. Nocera, *Tetrahedron Lett.*, 2006, **47**, 1923–1926.
26 V. Mirkhani, M. Moghadam, S. Tangestaninejad, B. Bahramian and A. Mallekpoor-Shalamzari, *Appl. Catal., A*, 2007, **321**, 49–57.
27 G. Consiglio, I. P. Oliveri, S. Cacciola, G. Maccarrone, S. Failla and S. Di Bella, *Dalton Trans.*, 2020, **49**, 5121–5133.
28 P. Kumar Mudi, A. Das, N. Mahata and B. Biswas, *J. Mol. Liq.*, 2021, **340**, 117193–117203.
29 M. Asadniaye Fardjahromi, M. Moghadam, S. Tangestaninejad, V. Mirkhani and I. Mohammadpoor-Baltork, *J. Iran. Chem. Soc.*, 2017, **14**, 1317–1323.
30 M. Balas, S. Beaudoin, A. Proust, F. Launay and R. Villanneau, *Eur. J. Inorg. Chem.*, 2021, **2021**, 1581–1591.
31 V. Mahdavi, M. Mardani and M. Malekhosseini, *Catal. Commun.*, 2008, **9**, 2201–2204.
32 J. Tong, Y. Zhang, Z. Li and C. Xia, *J. Mol. Catal. Chem.*, 2006, **249**, 47–52.

33 D. Zhu, Y. Chen, Y. Zhu, C.-Y. Liu, Q. Yan, X. Wu, K. Ling, X. Zhang, P. M. Ajayan, T. P. Senftle and R. Verduzco, *Macromolecules*, 2024, **57**, 1038–1049.
34 Y. Zhu, Y. Liu, Q. Ai, G. Gao, L. Yuan, Q. Fang, X. Tian, X. Zhang, E. Egap, P. M. Ajayan and J. Lou, *ACS Mater. Lett.*, 2022, **4**, 464–471.
35 C. Chung, Y.-K. Kim, D. Shin, S.-R. Ryoo, B. H. Hong and D.-H. Min, *Acc. Chem. Res.*, 2013, **46**, 2211–2224.
36 A. N. Ghulam, O. A. Dos Santos, L. Hazeem, B. Pizzorno Backx, M. Bououdina and S. Bellucci, *J. Funct. Biomater.*, 2022, **13**, 77–105.
37 D. Chen, H. Feng and J. Li, *Chem. Rev.*, 2012, **112**, 6027–6053.
38 K. Jiao, X. Wang, Y. Wang and Y. Chen, *J. Mater. Chem. C*, 2014, **2**, 7715–7721.
39 K. P. Loh, Q. Bao, G. Eda and M. Chhowalla, *Nat. Chem.*, 2010, **2**, 1015–1024.
40 P. W. Sayyad, S. S. Khan, N. N. Ingle, G. A. Bodkhe, T. Al-Gahouari, M. M. Mahadik, S. M. Shirsat and M. D. Shirsat, *Appl. Phys. A*, 2020, **126**, 1–8.
41 H. Su, S. Wu, Z. Li, Q. Huo, J. Guan and Q. Kan, *Appl. Organomet. Chem.*, 2015, **29**, 462–467.
42 G. Bian, P. Jiang, F. Wang, Y. Shen, K. Jiang, L. Liu and W. Zhang, *New J. Chem.*, 2018, **42**, 85–90.
43 A. Zarnegaryan, Z. Pahlevanneshan, M. Moghadam, S. Tangestaninejad, V. Mirkhani and I. Mohammdpoor-Baltork, *J. Iran. Chem. Soc.*, 2019, **16**, 747–756.
44 S. Rayati, E. Khodaei, S. Shokoohi, M. Jafarian, B. Elmi and A. Wojtczak, *Inorg. Chim. Acta*, 2017, **466**, 520–528.
45 M. Masteri-Farahani and M. Ghahremani, *J. Phys. Chem. Solids*, 2019, **130**, 6–12.
46 H. M. A. Hassan, M. A. Betiha, E. A. El-Sharkawy, R. F. M. Elshaarawy, N. B. El-Assy, A. A. Essawy, A. M. Tolba and A. M. Rabie, *Colloids Surf. A Physicochem. Eng. Asp.*, 2020, **591**, 124520–124531.
47 B. Rezazadeh, A. R. Pourali, A. Banaei and H. Behniafar, *J. Coord. Chem.*, 2019, **72**, 3401–3416.
48 S. R. Pour, A. Abdolmaleki and M. Dinari, *J. Mater. Sci.*, 2019, **54**, 2885–2896.
49 R. Hajian and E. Bahrami, *Catal. Lett.*, 2021, **152**, 2445–2456.
50 R. Hajian and A. Ehsanikhah, *Chem. Phys. Lett.*, 2018, **691**, 146–154.
51 R. Hajian, *Inorg. Chem. Res.*, 2021, **6**, 1–9.
52 D. Chen and A. Martell, *Inorg. Chem.*, 1987, **26**, 1026–1030.
53 D. C. Marcano, D. V. Kosynkin, J. M. Berlin, A. Sinitskii, Z. Sun, A. Slesarev, L. B. Alemany, W. Lu and J. M. Tour, *ACS Nano*, 2010, **4**, 4806–4814.
54 H. Su, Z. Li, Q. Huo, J. Guan and Q. Kan, *RSC Adv.*, 2014, **4**, 9990–9996.
55 S. Tangestaninejad, M. Moghadam, V. Mirkhani, I. Mohammadpoor-Baltork and M. S. Saeedi, *Appl. Catal., A*, 2010, **381**, 233–241.
56 S. Choudhary, H. P. Mungse and O. P. Khatri, *J. Mater. Chem.*, 2012, **22**, 21032–21039.
57 B. S. Lane, M. Vogt, V. J. DeRose and K. Burgess, *J. Am. Chem. Soc.*, 2002, **124**, 11946–11954.
58 K. K. Krishnan, A. M. Thomas, K. S. Sindhu and G. Anilkumar, *Tetrahedron*, 2016, **72**, 1–16.